RSC Advances

PAPER

View Article Online
View Journal | View Issue

Cite this: *RSC Adv.*, 2018, **8**, 21658

Facile morphology control of 3D porous CeO_2 for CO oxidation†

Xia Jiang, Xiaochun Huang, Wei Zeng, Jiale Huang, Yanmei Zheng, Daohua Sun* and Qingbiao Li*

Received 25th April 2018
Accepted 6th June 2018

DOI: 10.1039/c8ra03555e

rsc.li/rsc-advances

3D porous CeO_2 with various morphologies was successfully synthesized *via* a facile precipitation using glycine as the soft bio-template. During the synthesis, it was demonstrated that the morphology of CeO_2 depended on the molar ratio of reactants. Furthermore, the catalytic performance towards CO oxidation of the as-synthesized CeO_2 with different morphologies was investigated. CeO_2 with a bowknot shape showed excellent catalytic performance, giving complete CO conversion at 370 °C, due to its properties of much higher oxygen vacancies, loosely packed pore structure and larger specific surface area.

Introduction

CeO_2 has the most widespread applications in catalysis owing to its excellent oxygen storage capacity.[1,2] It has been proved that the morphology of CeO_2 could influence its catalytic performance to a certain extent. Specifically, the 3D structure of CeO_2 possesses remarkable advantages compared to 2D or 1D CeO_2 samples.[3] Thus, it is of great significance to obtain 3D porous CeO_2 materials with various shapes.

Numerous methods for synthesis of 3D porous CeO_2 with different morphologies have been developed, including spray pyrolysis,[4] precipitation methods,[5,6] combustion synthesis,[7] hydrothermal methods,[8–10] *etc.* However, among these methods, hazardous reagents and a series of energy consuming and tedious manipulations are usually needed. Again, it is difficult to obtain different morphologies of CeO_2 in the same preparation route. Hence, it is still a challenge to develop a facile process to synthesize 3D porous CeO_2 with different types of morphologies.

The bio-template method is one of the common synthesis strategies to prepare porous materials.[11] To date, diatom,[12] butterfly,[13] wood,[14] leaf,[15] cotton[16] and pollen[17] *etc.* are used as hard biotemplate to prepare kinds of porous materials. Qian reported that porous CeO_2 was obtained through a bio-template of lotus pollen.[18] However, this method was difficult to tune the pore structure and morphology of CeO_2, for the reason that the structure of the templates was natural and inherent. Amine acid, with the special structure of $-NH_2$ and –COOH, has been used in fabricating porous materials.[19,20] Among the numerous amine acids, glycine is the simplest in the structure. Moreover, Guo reported that amine acid with 2 carbon atoms (such as glycine) led to more loosely packed material, while the amine acid with more complicated structure and more carbons usually resulted in the close-packed products.[20] The loosely packed material owns more slit holes, which could increase the ability of mass transfer in catalysis.

Herein, a simple and soft bio-template of glycine was chosen to direct the growth of CeO_2 by a milder precipitation method in this work. We obtained 3D porous CeO_2 (A-CeO_2) with different morphologies by facilely changing the preparation conditions. Furthermore, the model reaction of CO oxidation was used to evaluate the influence of the structure of CeO_2.

Experimental

Urea, glycine, anhydrous ethanol, and cerium nitrate ($Ce(NO_3)_3 \cdot 6H_2O$) were analytical grade, and used as received. A-CeO_2 was prepared as following: 3.50 g $Ce(NO_3)_3 \cdot 6H_2O$ and 1.44 g urea were dissolved in 200 mL deionized water under vigorous stirring at room temperature, then 1.20 g glycine was added. After stirring for another 1 h, the solution was transferred to drying oven heated at 100 °C for certain time. Finally, the sample was dried and calcined at 500 °C in air. The obtained product is denoted as A-CeO_2 (3 : 2 : 1), the proportion in brackets is the molar ratio of urea, glycine and cerium nitrate. Different molar ratio of reactants for A-CeO_2 was prepared under the same reaction condition. The CeO_2 bulk was prepared by calcining $Ce(NO_3)_3 \cdot 6H_2O$ at 600 °C directly.

Functional groups of A-CeO_2 samples were investigated by Fourier transform infrared spectroscopy (FTIR, Nicolet 6700, USA). The crystal phases were obtained on X-ray powder diffraction (XRD, RigakuUltima IV, Japan). The UV-vis diffuse reflectance spectral (UV-vis DRS, Varian Cary 5000, USA) characterization was employed to calculate the band gap energy of samples. The thermo-gravimetric analysis (TGA, SDT Q600,

Department of Chemical and Biochemical Engineering, College of Chemistry and Chemical Engineering, Xiamen University, Xiamen, 361005, P. R. China. E-mail: sdaohua@xmu.edu.cn; kelqb@xmu.edu.cn

† Electronic supplementary information (ESI) available. See DOI: 10.1039/c8ra03555e

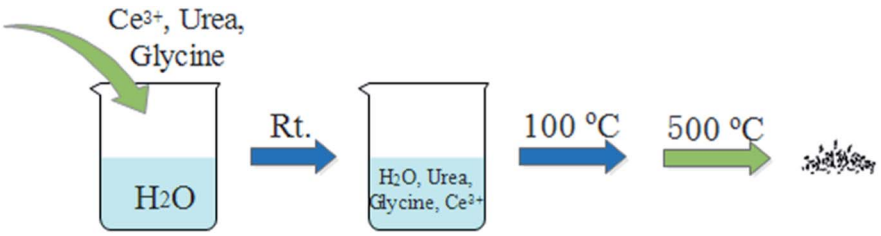

Fig. 1 Scheme of the synthesis of A-CeO_2.

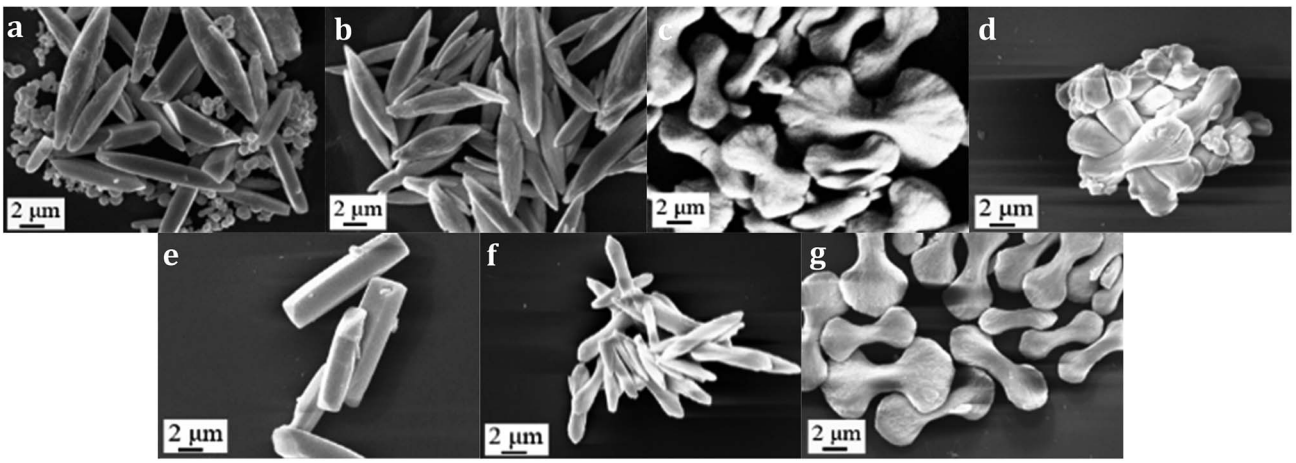

Fig. 2 SEM of A-CeO_2 with different reactants ((a) A-CeO_2 (3 : 0 : 1); (b) A-CeO_2 (3 : 1 : 1); (c) A-CeO_2 (3 : 2 : 1); (d) A-CeO_2 (3 : 4 : 1); (e) A-CeO_2 (1.5 : 2 : 1); (f) A-CeO_2 (6 : 2 : 1); (g) A-CeO_2 (3 : 2 : 2) the proportion in brackets is the molar ratio of urea, glycine and cerium nitrate).

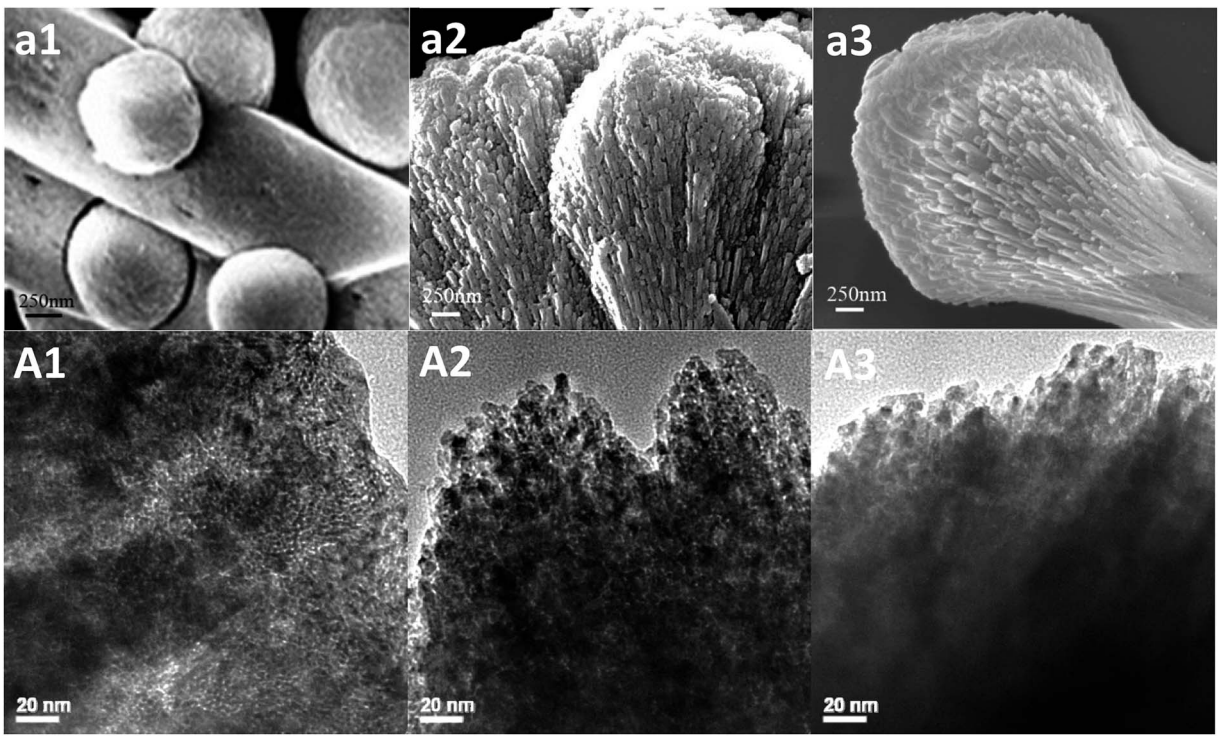

Fig. 3 SEM and TEM of special A-CeO_2 ((a1 and A1) A-CeO_2 (3 : 0 : 1); (a2 and A2) A-CeO_2 (3 : 2 : 1); (a3 and A3) A-CeO_2 (3 : 2 : 2) the proportion in brackets is the molar ratio of urea, glycine and cerium nitrate).

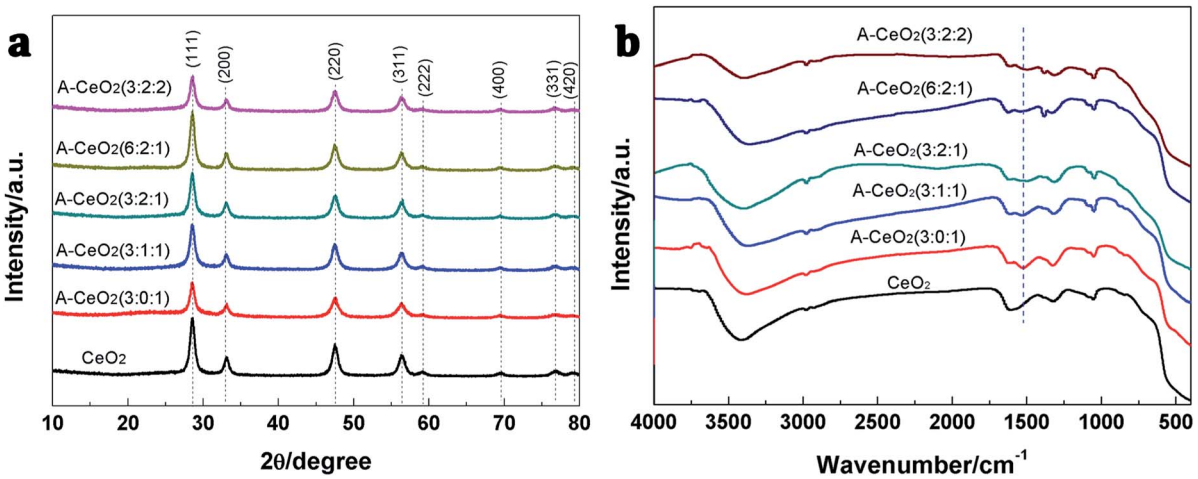

Fig. 4 XRD pattern (a) and FTIR spectra (b) of different A-CeO_2 samples.

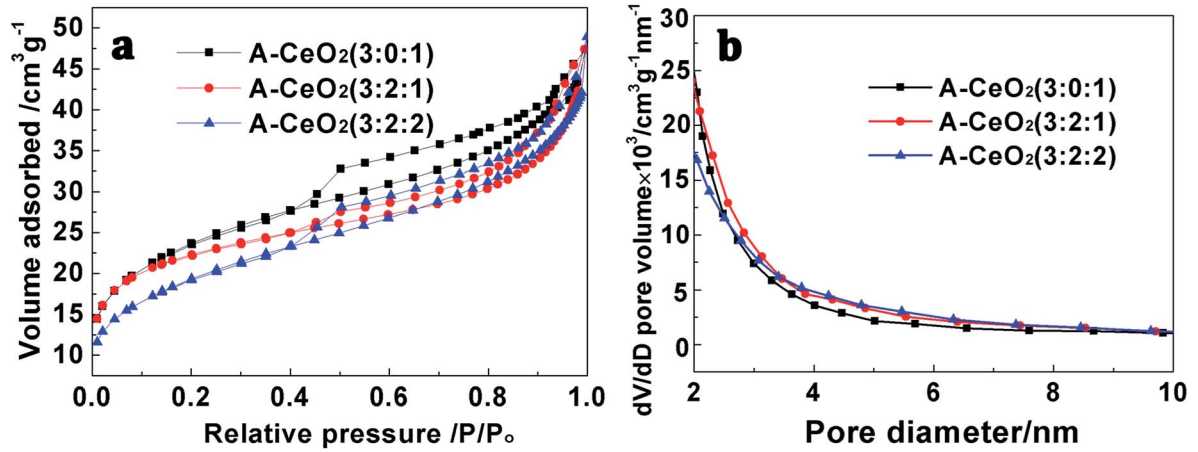

Fig. 5 N_2 adsorption–desorption isotherms (a) and corresponding pore size distribution curves (b) of different A-CeO_2 with different ratio of reactant.

USA) performed the thermal behavior of A-CeO_2. Morphologies of the samples were taken by scanning electron microscope (SEM, ZEISS SIGMA, Germany) and TEM (TECNAI F30, USA). Surface area and pore were characterized by N_2 adsorption/desorption measurements (BET, Tristar II3020, USA), pore size was calculated by the Barrett–Joyner–Halenda (BJH) model. Raman analysis (Renishaw, INvia) for detecting the oxygen vacancy was performed using a 532 nm excitation laser. The Ce valence state was detected by XPS (Physical Electronics, USA) using a monochromated Al Kα (1486.7 eV) as X-ray source in which the binding energy was calibrated with C 1s 284.8 eV. The H_2-TPR was used to illustrate the reducibility of samples.

The CO oxidation was carried out under atmospheric pressure in a fixed bed reactor containing 0.1 g catalyst. The reactor stream was composition of CO (1%), O_2 (1%) and Ar (98%) with the total flow rate of 20 000 mL h^{-1} g_{cat}^{-1}. The reactants and products analysis were investigated by gas chromatography (GC 9560) with a thermal conductivity detector.

Results and discussion

A-CeO_2 was prepared as illustrated in Fig. 1. $Ce(NO_3)_3 \cdot 6H_2O$, urea and glycine were dissolved in deionized water under vigorous stirring at room temperature for a certain time, then the solution was transferred to drying oven heated at 100 °C. Finally, the sample was dried and calcined at 500 °C (according to Fig. S1†) in air. The preparation was easy to implement, and we could obtain various morphologies of A-CeO_2 by simply changing the molar ratio of reactants (urea, glycine and cerium nitrate). As shown in Fig. 2, A-CeO_2 with about 10 μm spindle

Table 1 The properties and performance of A-CeO_2

Samples	E_g (eV)	Area R_{Ce-O}/area F2g (%)	S_{BET} (m^2 g^{-1})	T_{100} (°C)
CeO_2	2.67	5.91	—	620
A-CeO_2 (3 : 0 : 1)	2.63	6.88	78	480
A-CeO_2 (3 : 2 : 1)	2.48	8.74	85	370
A-CeO_2 (3 : 2 : 2)	2.47	7.38	70	480

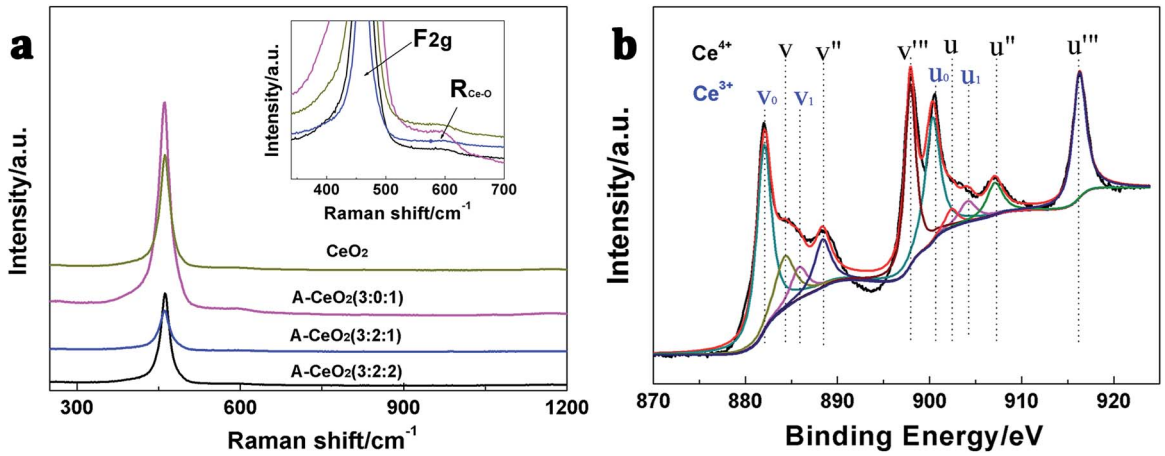

Fig. 6 Raman spectra (a) of CeO_2 and different A-CeO_2 with different ratio of reactant and Ce 3d core level XPS pattern (b) of A-CeO_2 (3 : 2 : 1).

structure and a few spherical particles were obtained without introducing glycine (Fig. 2a). As the increase of glycine, the spherical particles disappeared (Fig. 2b), further increasing mole ratio of glycine, the morphology of A-CeO_2 changed to bowknot (Fig. 2c) and bulk shape (Fig. 2d). Simply, the existence of glycine brought more uniform structure of A-CeO_2, and the amount of glycine influenced the morphology of A-CeO_2. The amount of urea and Ce precursor also affected the structure of A-CeO_2. A-CeO_2 (1.5 : 2 : 1) showed the prism shape (Fig. 2e), A-CeO_2 (6 : 2 : 1) performed small dumbbell shape (Fig. 2f), and A-CeO_2 (3 : 2 : 2) presented dumbbell shape (Fig. 2g). In Fig. 3, Enlarged Fig. 2 and TEM of special samples showed that different shapes owned different stack forms. It was no obvious stack when without glycine (Fig. 3a1 and A1). A-CeO_2 (3 : 2 : 1) showed the stack form of sticks that was linked by balls. However, A-CeO_2 (3 : 2 : 2) piled in prismatic forms.

As shown in Fig. 4a, the prepared A-CeO_2 had the same structure of cubic fluorite with face centered as CeO_2 (JCPDS file no. 34-0394).[2] Meanwhile, there were no other crystalline byproducts and obvious difference in characteristic diffraction peaks could be observed, confirming the high purity among various morphologies. In FTIR spectra (Fig. 4b), different morphologies of A-CeO_2 showed basically consistence, but the obtained A-CeO_2 exhibited a –NH flexural vibration at about 1522 cm^{-1} compared with CeO_2, indicating that the addition of glycine could residual N element. Nitrogen adsorption–desorption isotherms of special samples (Fig. 5a) corresponded to the type IV curves with H3 hysteresis loop, that reflected the A-CeO_2 owned the feature of slit mesoporous (2–4 nm, Fig. 5b). And, the samples exhibited similar pore size distribution rule. Different morphologies presented different specific surface areas (Table 1), and A-CeO_2 (3 : 2 : 1) owned the larger specific surface areas of 85 m^2 g^{-1}. Hence, the 3D porous A-CeO_2 with tuning morphology was successfully obtained *via* a milder process. The whole preparation process is more economic than the previous report by Mitchell and coworkers.[21]

As we all know that oxygen vacancies dominate the electronic and chemical properties of CeO_2.[2] In this work, Raman (Fig. 6a) and XPS (Fig. 6b and S3†) were used to exhibit the concentration of oxygen vacancies. According to the report,[22] the typical Raman shift at 460 cm^{-1} and 600 cm^{-1} can be assigned to F2g vibration of the fluorite-type structure and oxygen vacancies. More importantly, the integral area ratios of oxygen vacancy peak (R_{Ce-O}) and F2g reflect the oxygen vacancy concentration. As shown in Table 1, A-CeO_2 (3 : 2 : 1) had the larger oxygen vacancy concentration, and relatively narrower energy gap (E_g) (Fig. S2† and Table 1) further verified the higher oxygen vacancy concentration of A-CeO_2 (3 : 2 : 1). The XPS spectra were used to study the valence state of Ce/oxygen vacancies of CeO_2 and *etc.* As shown in Fig. 6b and S3,† the Ce 3d spectrum of samples showed the appearance of the v, v″, v‴, u, u″ and u‴, which were attributed to Ce^{4+}. The v_0, v_1, u_0 and u_1 peaks were characteristic peaks of Ce^{3+}.[23] Moreover, the Ce^{3+}/Ce^{4+} of CeO_2, A-CeO_2 (3 : 0 : 1), A-CeO_2 (3 : 2 : 1) and A-CeO_2 (3 : 2 : 2) were 0.837, 0.857, 0.888 and 0.873 respectively. It was known that the higher Ce^{3+} concentration in nanoparticles was correlated with higher oxygen vacancy, so the obtained A-CeO_2 owned more oxygen vacancy than CeO_2, and A-CeO_2 (3 : 2 : 1) exhibited the highest oxygen vacancy concentration, that coincided with the results of the Raman spectra.

The H_2-TPR profiles (Fig. 7) showed that all the samples owned a broad profile centered around 500 °C corresponding to

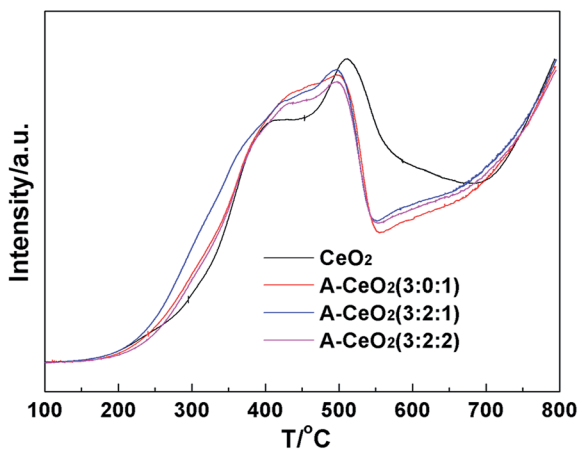

Fig. 7 The H_2-TPR profiles of CeO_2 and different A-CeO_2 with different ratio of reactant.

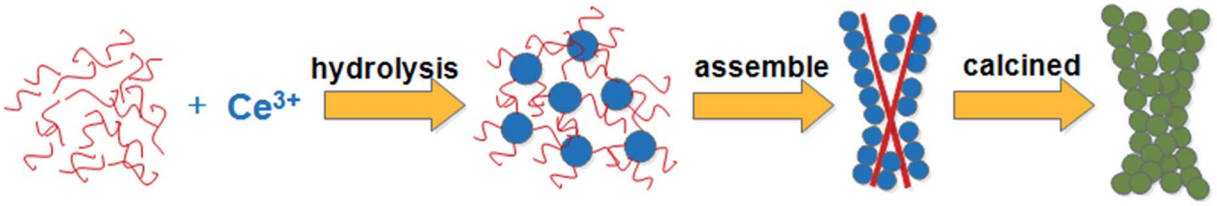

Fig. 8 Schematic illustration for the formation process of A-CeO_2.

the consumption of surface oxygen species and a high-temperature reduction peak above 800 °C arose from bulk reduction.[23] The peak characteristic of surface oxygen species at lower temperature of A-CeO_2 indicated that the synthesized nanomaterials possessed relatively stronger surface activity, and A-CeO_2 (3 : 2 : 1) exhibited the strongest surface activity.

The formation process of typical A-CeO_2 was investigated by FTIR, SEM and XRD. Fig. S4a† showed the FTIR spectra of the reactants and products. It could be inferred that glycine acted as a complexing agent in the reaction. Urea was supposed to be a precipitant due to the phenomenon of more A-CeO_2 formation as increasing the dosage of urea (Table S1†). The molar ratio of reactants could influence the dispersion and hydrolysis rate of Ce^{3+}, and then affect the morphology of A-CeO_2. The adsorbed Ce^{3+} hydrolyzed on the surface of glycine, and then the sphere $CeCO_3OH$ (Fig. S4b,† orthorhombic structure, JCPDS file no. 41-0013) was formed. In order to further verify the sphere structure, addition of ethanol in the solvent to prevent from the hydrolysis of Ce^{3+}, and then decrease the formation rate of A-CeO_2,[3] the obtained sample was sphere nanoparticle (Fig. S5†). Moreover, the shape of A-CeO_2 changed from sphere, bowknot to bulk over time (Fig. S6†). Above all, we supposed the schematic diagram as shown in Fig. 8.

The catalytic effect for CO oxidation of typical A-CeO_2 with different morphologies was investigated. Fig. 9 showed that the catalytic performance was highly dependent on the shape of A-CeO_2, and the complete CO conversion temperature of A-CeO_2 (3 : 2 : 1) was 370 °C, which was much lower than others especially the CeO_2 (620 °C) in bulk (Fig. S7†). The catalytic performance was also better than the reported commercial CeO_2 powers, CeO_2 nanowires and 3D ordered macroporous CeO_2.[5,6,24] The A-CeO_2 (3 : 2 : 1) with bowknot shape showed the best catalytic effect might be due to its outstanding features: higher oxygen vacancy (Table 1) for improving oxygen mobility,[24] more loosely packed porous structure (Fig. 4d) and larger specific surface area (Table 1), which could intensify mass transfer.[7]

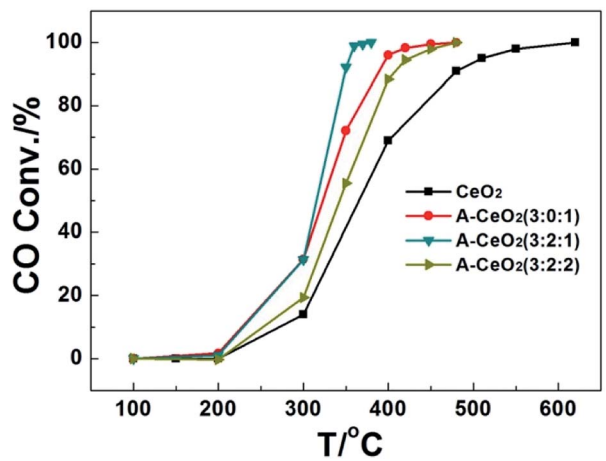

Fig. 9 CO oxidation evaluation of different CeO_2.

Conclusions

In summary, a series of A-CeO_2 with different morphologies, namely spindle, bowknot, dumbbell and prism, have been successfully fabricated *via* a milder precipitation route assisted by glycine. The catalytic performance for CO oxidation of the as-synthesized A-CeO_2 is strongly dependent on the shape of A-CeO_2. Owing to the outstanding properties, A-CeO_2 (3 : 2 : 1) with bowknot shape possesses the excellent catalytic activity with the complete CO conversion temperature of 370 °C. The facile and eco-friendly synthesis method of A-CeO_2 may provide reference for the preparation of other 3D porous metal oxides. The prepared CeO_2 with different microstructures is promising for the future practical application in catalysis.

Conflicts of interest

There are no conflicts to declare.

Acknowledgements

Authors are thankful for the financial support of National Natural Science Foundation of China (21536010 and 41773105) and Natural Science Foundation of Fujian Province (2017J01025)

Notes and references

1 T. Montini, M. Melchionna, M. Monai and P. Fornasiero, *Chem. Rev.*, 2016, **116**, 5987–6041.
2 C. Sun, H. Li and L. Chen, *Energy Environ. Sci.*, 2012, **5**, 8475.
3 H. Liu and H. Liu, *J. Alloys Compd.*, 2016, **681**, 342–349.
4 S.-J. Shih, W.-L. Tzeng and W.-L. Kuo, *Surf. Coat. Technol.*, 2014, **259**, 302–309.
5 X. Lu, X. Li, J. Qian and Z. Chen, *Powder Technol.*, 2013, **239**, 415–421.
6 G. Mu, C. Liu, Q. Wei and Y. Huang, *Mater. Lett.*, 2016, **181**, 161–164.
7 W. Kang and A. Varma, *Appl. Catal., B*, 2018, **220**, 409–416.

8 C. Cheng, F. Chen, H. Yi and G. Lai, *J. Alloys Compd.*, 2017, **694**, 276–281.
9 B. Zong, *J. Mater. Sci.: Mater. Electron.*, 2016, **28**, 2458–2461.
10 X. Niu, M. Li, B. Hao and H. Li, *J. Mater. Sci.: Mater. Electron.*, 2016, **27**, 6845–6848.
11 X. Y. Yang, L. H. Chen, Y. Li, J. C. Rooke, C. Sanchez and B. L. Su, *Chem. Soc. Rev.*, 2017, **46**, 481–558.
12 D. Liu, J. Gu, Q. Liu, Y. Tan, Z. Li, W. Zhang, Y. Su, W. Li, A. Cui, C. Gu and D. Zhang, *Adv. Mater.*, 2014, **26**, 1229–1234.
13 Z. He, W. Zhang, W. Wang, M. Tassin, J. Gu, Q. Liu, S. Zhu, H. Su, C. Feng and D. Zhang, *J. Mater. Chem. B*, 2013, **1**, 1673.
14 J. Xi, E. Zhou, Y. Liu, W. Gao, J. Ying, Z. Chen and C. Gao, *Carbon*, 2017, **124**, 492–498.
15 H. Zhou, X. Li, T. Fan, F. E. Osterloh, J. Ding, E. M. Sabio, D. Zhang and Q. Guo, *Adv. Mater.*, 2010, **22**, 951–956.
16 D. Shen, Y. Dai, J. Han, L. Gan, J. Liu and M. Long, *Chem. Eng. J.*, 2018, **332**, 563–571.
17 K. Tian, X.-X. Wang, H.-Y. Li, R. Nadimicherla and X. Guo, *Sens. Actuators, B*, 2016, **227**, 554–560.
18 J. Qian, Z. Chen, C. Liu, X. Lu, F. Wang and M. Wang, *Mater. Sci. Semicond. Process.*, 2014, **25**, 27–33.
19 A. F. Alkaim, E. M. Alrobayi, A. M. Algubili and A. M. Aljeboree, *Environ. Technol.*, 2017, **38**, 2119–2129.
20 Y. Guo, S. Lin, X. Li and Y. Liu, *Appl. Surf. Sci.*, 2016, **384**, 83–91.
21 S. L. Mitchell and J. Guzman, *Mater. Chem. Phys.*, 2009, **114**, 462–466.
22 B. Xu, Q. T. Zhang, S. S. Yuan, M. Zhang and T. Ohno, *Chem. Eng. J.*, 2015, **260**, 126–132.
23 T. S. Sreeremya, A. Krishnan, K. C. Remani, K. R. Patil, D. F. Brougham and S. Ghosh, *ACS Appl. Mater. Interfaces*, 2015, **7**, 8545–8555.
24 X. Zhou, J. Ling, W. Sun and Z. Shen, *J. Mater. Chem. A*, 2017, **5**, 9717–9722.